Chapter

Metalens Antennas in Microwave, Terahertz and Optical Domain Applications

Qi Song, Yan Gong, Nianxi Xu and Ruoqian Gao

Abstract

Metamaterial is the artificial structure under sub-wavelength dimension and could be designed to manipulate the electromagnetic wave radiation across the broad frequency range through microwave to much higher frequency, such as terahertz and optical regime. Lens antenna can generate the focused beam with high gain and shrink the bulky refractive body and feeds into a shape of flat form. This chapter will discuss the general concepts of metalens and the technology of metalens-based antenna at microwave, terahertz and optical frequency. The recent progress in the research and development of metalens antennas is reviewed with designs principle and typical applications. At last part, some innovative techniques such as dynamic focus-tuning of metalen are discussed in details.

Keywords: Microwave metalens antenna; Terahertz metalens, Optical metalens, achromatic metalens, metamaterial absorber

1. Introduction

Metamaterial is a specific type of artificial materials that is constructed with amount of sub-wavelength structure units and is able to realize the complex systems in a compact and planar configuration [1]. In the early stage, Metasurfaces with metal patterned surfaces have been used to achieve the desired phase-shift distribution for antenna design and EM wave manipulation in the microwave domain [2]. Among aperture antennas, lens has long been used in antenna design and lens antennas usually are electrically larger with volume constraints and the complex feeding structure. The conventional lens can be structured using dielectric lens and transmit-receive arrays. Metalens antennas provide much more flexibility of planar design and fabrication than the dielectric lenses, since it can realize spherical phase in the plane and replace the complex feeding structure with the waveguide or the novel coupler structure. Furthermore, the metalens also controls the amplitude and polarization direction of the incident electromagnetic wave, which is the most privilege advantage and the popular usage for most metalens applications [3]. Researchers have designed the high quality metasurface lens and beamforming on the grapheme terahertz metalens. Some traditional optical devices could be replaced by metasurface such as lens, gratings and prism [4]. The transformation optics has been employed to compress the sphere into a cylinder and the flat lens with a beam-steering by using cylindrical dielectric slabs. Such designs have been widely applied in 5G NR and radar systems [5]. If the unit cell of metalens is dynamically adjusted, the focus of metalens could be managed accordingly and the system could scan the beam in the space, which is the highly desired feature in the area of microwave band for 5G MIMO applications, terahertz communications and imaging, and modern optical imaging and sensing system, such as 3D microscope and LiDAR [6, 7].

2. Design principle

When electromagnetic wave propagates through the micro-structures, the wavefront shape of emergent wave is controlled by distributing the phase profile across the outputting surface. Generally, there are few steps to design a metalens. Firstly, the phase profile of the metalens aperture should be solved per desired. Secondly, the large amount of micro-structures is investigated to cover both the full phase variance and the dispersion at the same time. If the particular functionalities are needed, such as achromatic focusing, large numerical aperture (NA), the broader phase range is highly desired for the consideration of the dispersion margin as well. At last, the appropriate structures from the "phase library" is distributed accordingly to form the metalens, and the simulation of the whole metalens device with full wave simulator and experimental characterization are carried out to provide the full design circle of the metalens. The following parts will give the examples of typical metalens antenna applications with more design details.

2.1 Beam focalization and steering effect

In the traditional research of ultrasound and microwave domain, the concept of phased array antenna is introduced as a set of radiators with the designed phase and amplitude over the synthetic aperture. In order to simplify the design procedure and extend the possibility to more complex functionalities, the concept of the phased array model could be used here to explain the physics of the metalens [3]. For example, a focusing metalens could be recognized as the phased-array antenna with the special case of the spherical phase profile.

We assume the periodic metasurface could be regarded as a plane distributed with radiator array as shown in **Figure 1** to start a general discussion. In this case, the most common case of "lens" could be understood from the focalization effect, which of metalens could be achieved by distributing the spherical phase profile over the plane surface, as shown in Eq. (1) [4]. The wavefront generated by the phased array reach the focus at the same time, as shown in **Figure 1(b)**.

$$\varphi(x,y) = 2\pi - \frac{2\pi}{\lambda_d}\left(\sqrt{x^2+y^2+f^2} - f\right) \tag{1}$$

Starting from a general discussion, due to the periodicity of a phased array, beam narrow effect is invoked by the nature of the periodic array. The focalization effect only happens when the wavesfronts reach at the focus point simultaneously by spherical phase shift, as shown in **Figure 1(b)**. At the focus point, the maximum intensity is obtained as the result of the interference of each "meta-atom". The beam steering effect could be realized by adding the constant phase increment between two adjacent elements, as shown in **Figure 1(c)**. Furthermore, the steering

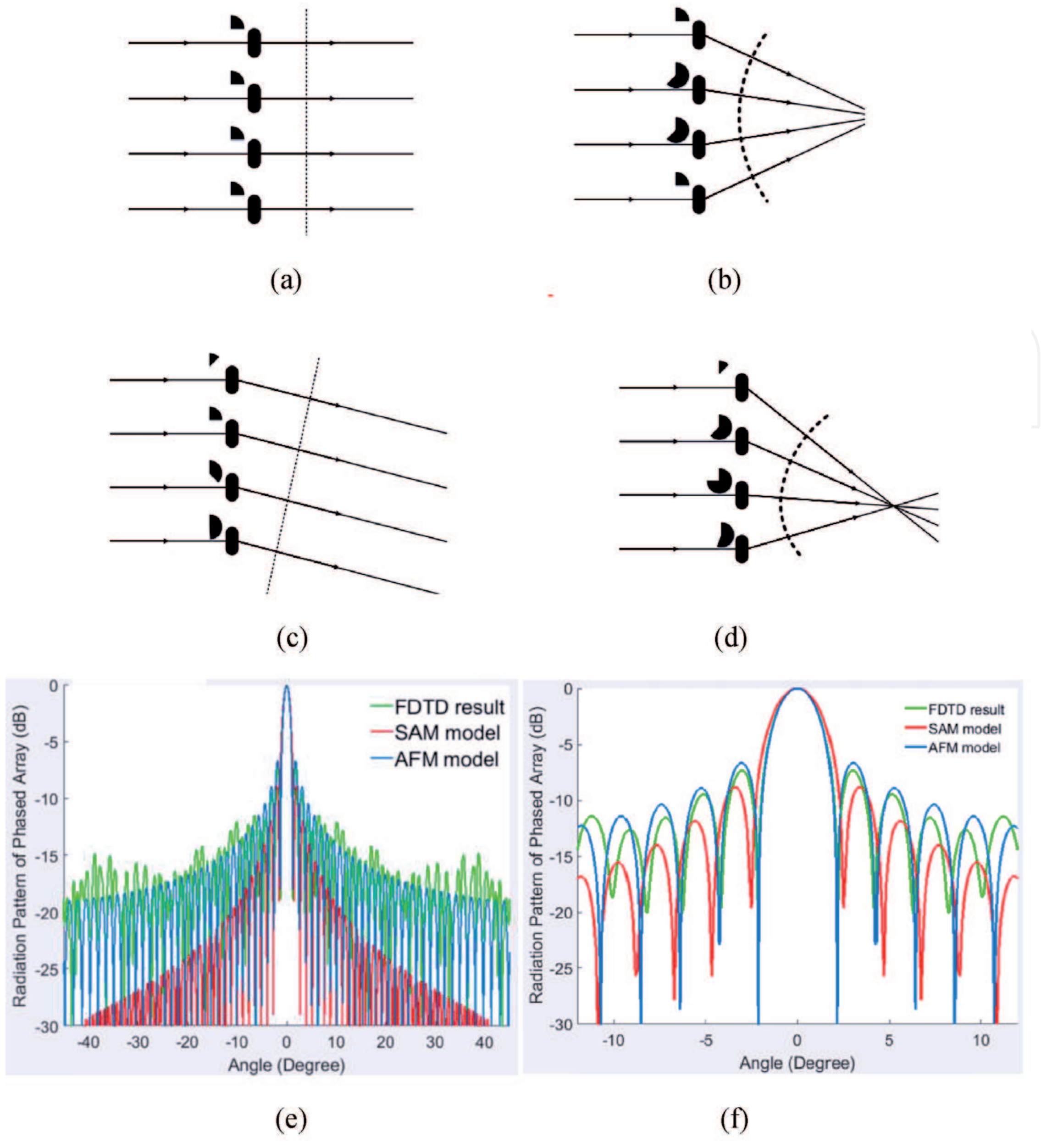

Figure 1.
(a) Focalization effect (b) beam narrowing effect (c) beam steering and (d) focus steering effects generated by a phased array surface. (e) the far-field radiation pattern of phased array of FDTD simulation, SAM and AFM model results and (f) the enlarged region of the maximum radiation peaks.

angle could be tuned by controlling the phase increment [3]. **Figure 1(d)** gives another instance of the combination of focusing and steering if the spherical phase shift and constant phase increment are added on top of the phase shift. Based on the phased array models described here, full-wave solver as FDTD simulator and analytical models, such as Synthetic Aperture Method (SAM) and Array Factor Method (AFM), are investigated to give the radiation pattern at far field. **Figure 1(e)** and **(f)** shows the far-field radiation patterns of the metalens model for optical frequency at 193THz, obtained by FDTD simulator, SAM model and (AFM) model respectively, which shows that the phased array models highly agree with the full-wave simulation result. Theoretically, the focalization and steering effects can be realized at the same time, which makes more advanced features highly possible, especially for tele-communication system by replacing the bulky scanning infrastructure and project the wavefront to desired location with speed up to hundreds mega-Hertz.

2.2 Building the phase library of unit-cell

There are two primary modes of metasurface from the unit-cell's viewpoint. One type of unit-cell could be treated as the truncated waveguide and the waveguide mode is excited accordingly. This model usually matches well for the case at high frequency, such as high terahertz and optical regime. Another is resonate mode which could be treated as resonating antenna array. In order to better understand the unit cell's phase variation behaviors in the sub-wavelength dimension and obtain the enough coverage for the potential design phase library, we analyze the waveguiding effect and resonance mode below.

2.2.1 Waveguiding effect

To gain a better insight into the phase realization mechanism, we calculated the phase imparted solely by the wave-guiding effect [5]. This phase is given by

$$\phi_{WG} = \frac{2\pi}{\lambda_d} n_{eff} H \tag{2}$$

where H is the height of nanopost. The effective index n_{eff} of the fundamental mode (HE_{11}) can be calculated from the model the step-index circular waveguide. **Figure 2(e)** indicates that the phase profile from this model follows the calculated result from the finite difference time domain (FDTD) simulation of the nanopost unit-cell on the glass substrate. The good agreement indicates that the confinement of the fundamental mode increases with the waveguide diameter. The average absolute phase difference between the wave-guiding effect and the full-wave analysis is less than π/6. This indicates that the wave-guiding effect is the mechanism dominating considering the practical phase realization. Therefore, as shown in the **Figure 2** below, the phase library can cover 2π by changing the diameter of the cylinder.

2.2.2 Resonance modes

Another major approach of metasurface is the V-shaped nano-antenna array, which consists of series of two pillared Ag strips connected at the ends with the designed angles. The V-shaped antenna unit has the unique property of double-resonating effect, which includes symmetric and asymmetric components. When a vertical polarized light incidents along x-direction to the nanoantenna array, the incident field can be divided into component E_s and component E_a which are perpendicular and parallel to antenna axis, respectively. Component E_s excites plasmonic symmetric mode while component E_a excites asymmetric one. The double-resonance mode enables V-shaped antenna to provide phase changes of 2π with the large amplitude [8]. The **Figure 3** shows that the resonance mode is changed by opening of the V shape to cover 2π.

3. Metalens applications

3.1 Metalens antenna for beamforming massive MIMO

Metamaterial is usually used to reduce the antenna size and mutual coupling of antenna array, increase the efficiency and bandwidth. In this applications, a

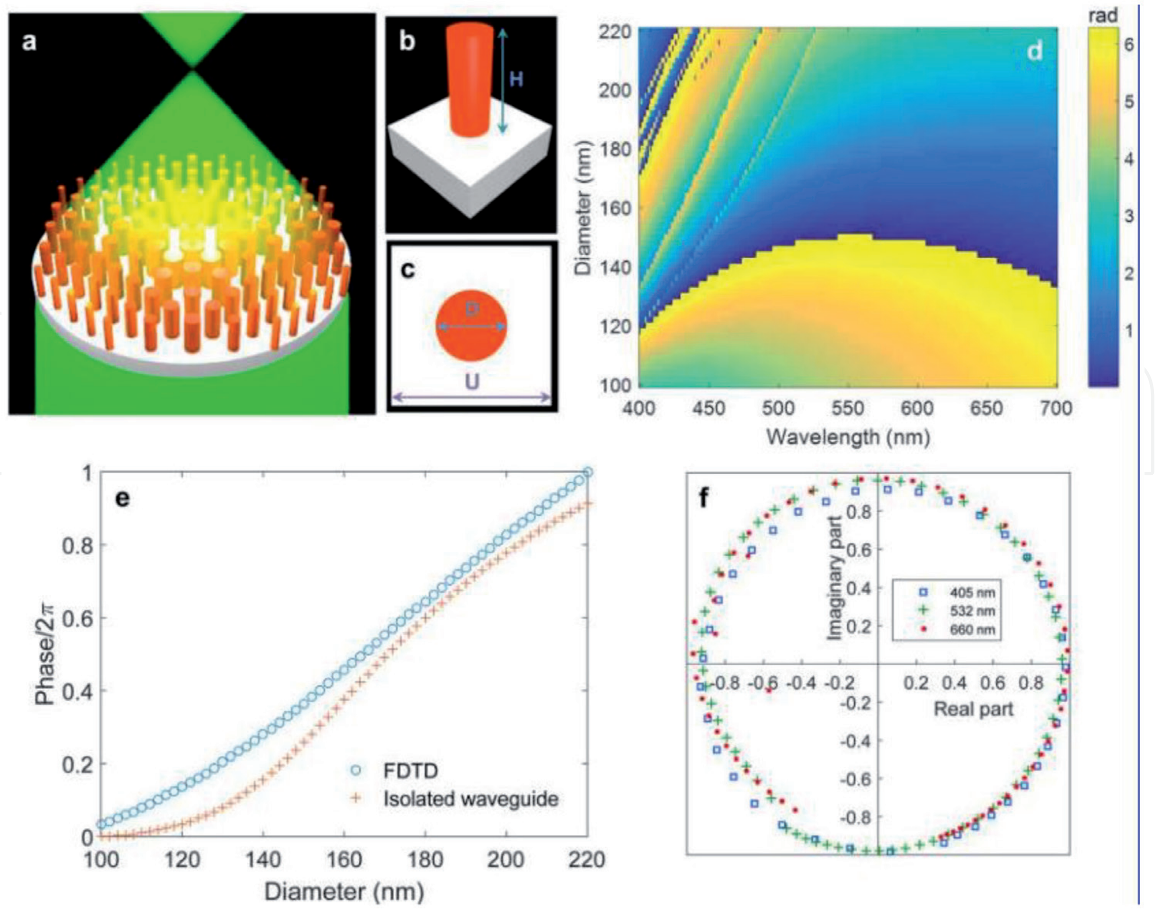

Figure 2.
(a) Schematic of a metalens operating in transmission mode. (b, c) Side-view and top-view of the metalens building lattice as a TiO_2 nanopillar on a glass substrate. For the design wavelength λ_d = 405 nm, 532 nm, 660 nm, the unit cell dimension is U = 180 nm, 250 nm, 350 nm, H = 400 nm, 600 nm, and D vary between 80 to 155 nm. (d) The phase map φ(D) of the metalens simulated at λ_d = 532 nm. The phase map represents the relative phase difference between the nanoposts and the reference point which there is no nanopost. (e) The phase comparison from FDTD simulation of the cell with varying diameter D, and the phase in the single cylindrical waveguide of the fundamental mode (HE_{11}) with the wavelength of 532 nm. (f) Transmission coefficients in complex space at three different wavelengths. The colored points show the amplitude and phase of the transmitted light of the nanopost.

metalens antenna with substrate integrated waveguide (SIW) feeding structure is present for low-cost broadband antenna for coming 5G massive MIMO applications at 28GHz, as shown in **Figure 4(a)**. **Figure 4(b)** shows that Jerusalem cross (JC) pattern is used as unit cell to form the metalens surface, where the width of JC unit p = 4.6 mm, c1 = 3.9 mm and c2 = 2.7 mm. A double-layer metalens structure is used to enhance the focusing effect and 7 feeding units are aligned to transmit or receive signal from different angles. Both the lens and feeding structure are fabricated with the regular printing circuit board (PCB) process. To scan the beam over the broad range from −25° to 25°, the array of SIW feeding stacked-patch antenna is used as the transmit/receive antenna from different angles. SIW structure in **Figure 4(c)** is often used for better confinement with minor loss above 20GHz. More design parameters could be found in **Table 1**. Metalens antenna could be excited by this feeding antenna mechanism or receive signal from certain angle individually. Finally, the measured results validate the design of the lens antenna well.

Generally, metalens antenna with angular feeding element could be used for the spatial beamforming and multi-beam 5G massive MIMO communication. **Figure 4(e)** shows that the planar lens has the stable focusing performances as well as linear beam scanning angle of ±25°. The arrangement and distance of feeding elements are analyzed on power distribution and the result shows that a linear

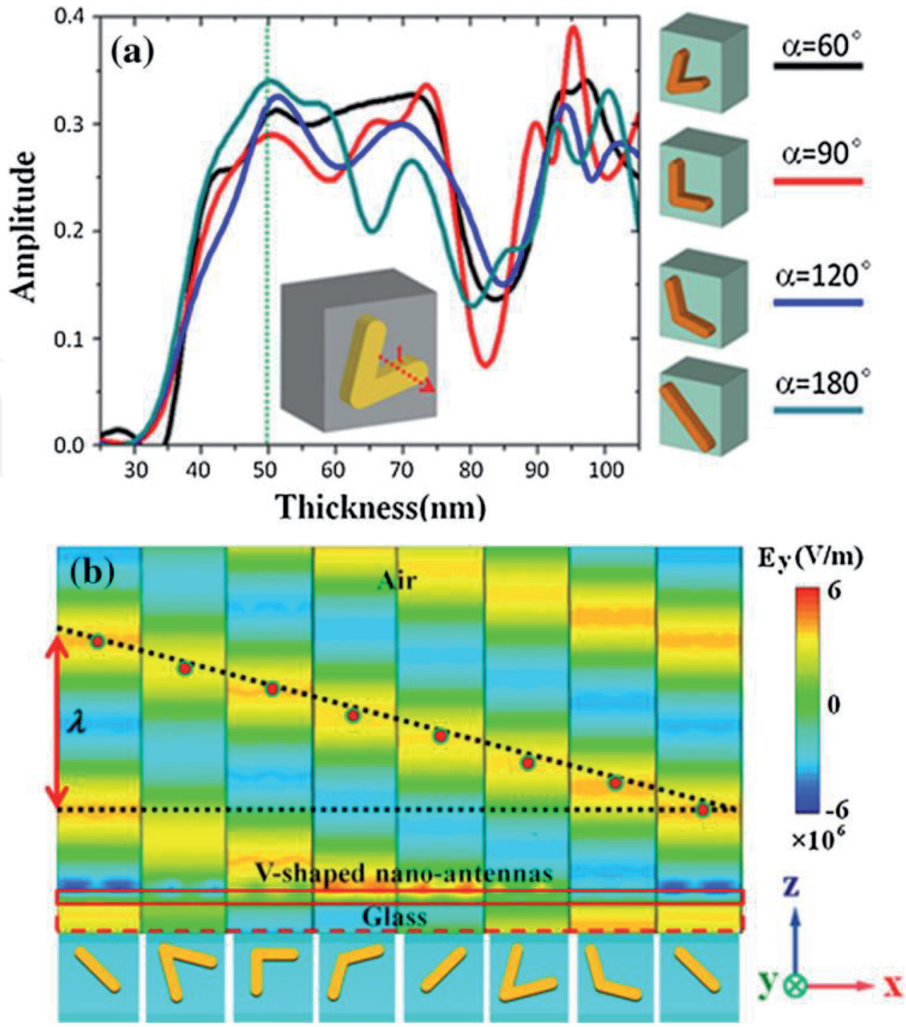

Figure 3.
Simulation of V-shaped antenna unit. (a) Curves of V-shaped nanoantenna amplitude variations as the antenna thickness t changes for the case of 60°, 90°, 120°, 180°, respectively. (b) Electric field distribution of cross-polarized light of 8 V-shaped nanoantenna.

uniformly feeding array could be placed accordingly to the scanning angle in free space. The antenna has the measured gain of 24.2 dBi, side lobe level (SLL) less than −18 dB compared to the center feeding port. Metalens antenna could deliver the constant radiation across 26–29 GHz and realizes a beamforming of ±25° with a gain tolerance of 3.7 dB through switching the ports of the feed elements. The lens and the feeding array have been verified easily fabricated by standard PCB procedure, which is promising for the future telecommunication and radar system applications.

3.2 Polarization devices based on the dielectric metasurface

In order to implement the high-efficiency polarization devices at the THz frequency, Si micro-brick arrays have been investigated in this design [9]. Since there is very low absorption loss for the silicon crystal around 1THz, the refractive index n and the dielectric constant å are 3.41 and 11.6. The anisotropic property with symmetric axes along x and y directions makes it possible to control x and y polarized field separately without the cross-polarization coupling effect. In this structure, Si micro-brick arrays are attached to the TPX substrate for the purpose of low absorption loss, the suitable refractive index matching, stable mechanical properties and the adhesion. The Si micro-brick unit with substrate is shown in **Figure 5**, where a double-phase modulation THz metasurface is based on the Si micro-bricks, in which the side length of the Si micro-bricks, L_x and L_y are

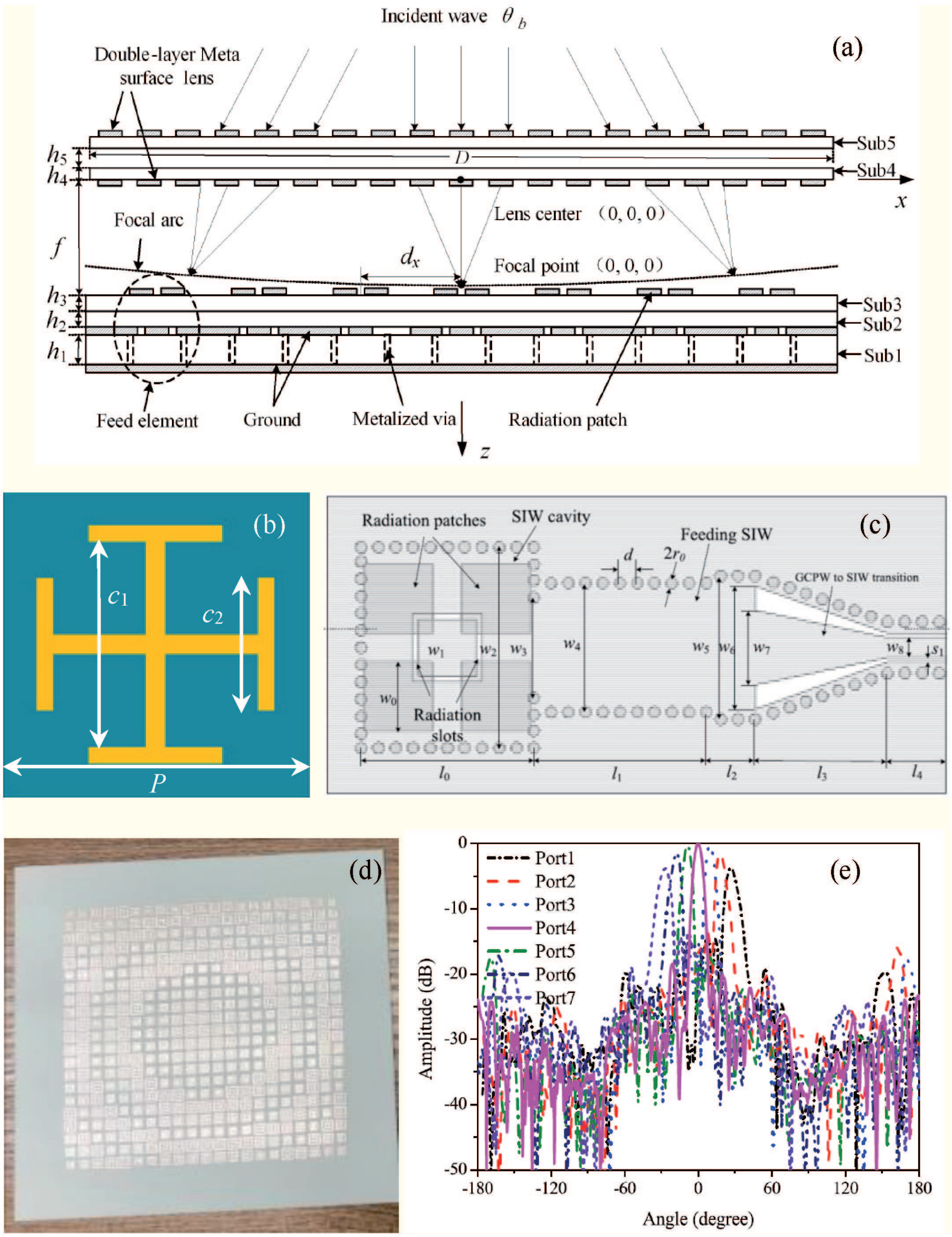

Figure 4.
(a) The skeptic view of metalens antenna with SIW feeding components from the bottom. (b) Jerusalem cross is used as the unit cell of metalens (c) tapered SIW with radiation patches are used for transmit/receive feeding array unit (d) Fabricated metalens with copper elements on the polymer substrate and (e) simulated radiation pattern with different incident angles in the focus plane.

Unit (mm)	
$w_0 = 2.4, w_1 = 2.2, w_2 = 7, w_3 = 3.5, w_4 = 4.5, w_5 = 5, w_6 = 4.3, w_7 = 2.6, w_8 = 0.7$	$l_0 = 6, l_1 = 6, l_2 = 1.7, l_3 = 4.6, l_4 = 1.8$
$h_1 = 0.813, h_2 = 0.202, h_3 = 0.508, h_4 = 0.203, h_5 = 1.52$	$s_1 = 0.15, d = 0.6, r_0 = 0.4, c_1 = 3.9, c_2 = 2.7, P = 4.6$

Table 1.
Design parameters used in MIMO Metalens antenna.

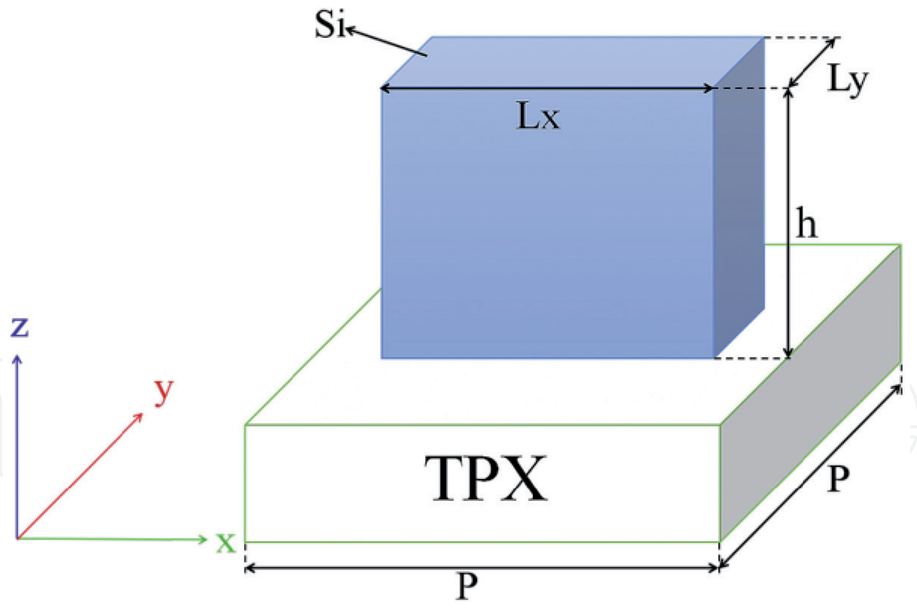

Figure 5.
The silicon micro-brick unit: P = 150 μm, h = 195 μm, Lx = 120 μm and Ly = 60 μm.

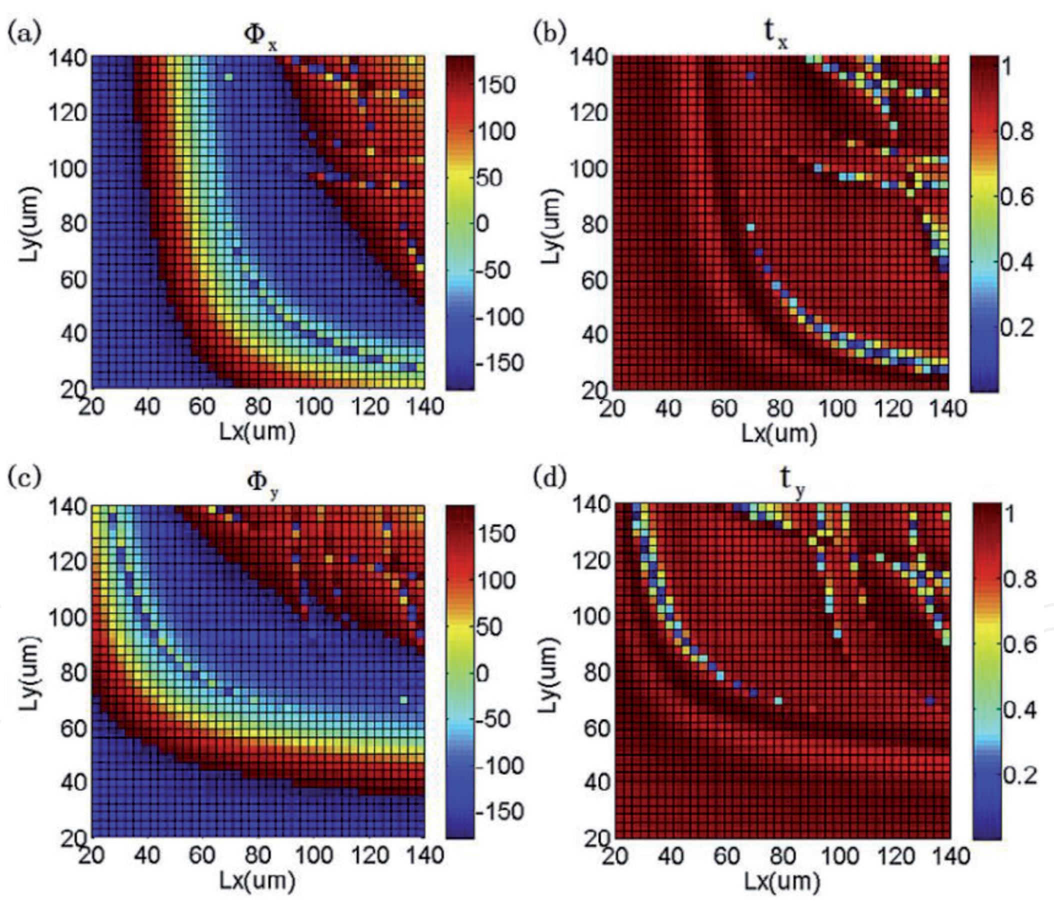

Figure 6.
Electromagnetic field presence of the Si micro-brick unit cell with Lx and Ly variations at 1.0 THz. The phase changes Φx (a) and transmission amplitude tx (b) of the Si unit as a function of Lx and Ly with the x-polarized incidence. The phase changes Φy (c) and transmission amplitude ty (d) as a function of Lx and Ly with the y-polarized incidence.

fine-tuned from 30 μm to 140 μm to match the desired electromagnetic profile. Si micro-bricks array is taken as homogeneous and of infinite extent in both in-plane dimensions. The transmitted phase shifts Φ_x, Φ_y and the transmittance t_x and t_y of the x, y-polarized light, are shown in **Figure 6(a–d)**. The simulated 2π phase

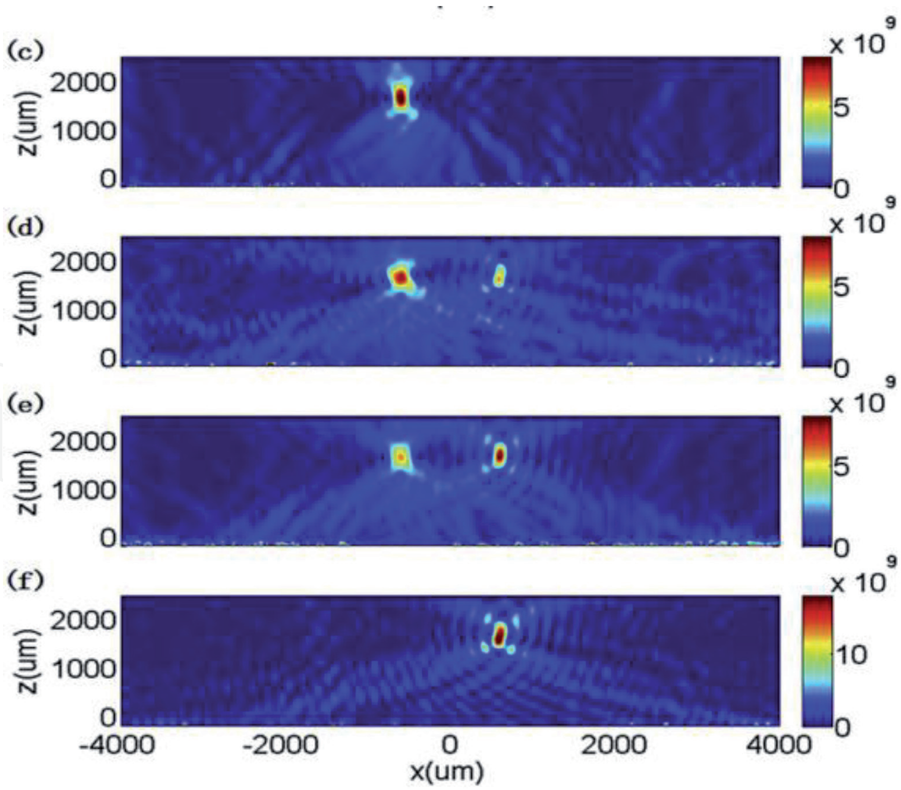

Figure 7.
The phase distribution of the designed DFM along the x direction for XLP (a) and YLP (b). The transmitted intensity distributions of the designed DFM under the XLP (c), 30° LP (d), 45° LP (e) and YLP (f) incidences respectively.

variations with transmission over 90% are shown in **Figure 6**. Nearly any combination of phase shifts from 0 to 2π with high transmittance for two polarizations can be obtained from single unit block by setting Lx and Ly properly. Conclusively, the double-phase modulation could be realized by the modulating two polarizations separately for this structure.

In **Figure 7(c)** and **(f)**, the XLP light will be focused to the left side position at $x = -x_0$; y = f. Parallelly, the YLP light will be focused to the right side position at $x = x_0$; y = f. In fact, any polarized light, such as the 30° LP and 45° LP, can be decomposed to x and y polarization components and be focused separately. If designing a dual-focus metalens, there will be two focus spots in the focal plane as shown in **Figure 7(d)** and **(e)**. 30° LP and 45° LP lights can be two focusing spots corresponding to the x and y-polarization. **Figure 7** shows that the focusing intensity of y-polarization component is increased with the LP angles, and the focus intensity of x-polarization component is decreased. The result shows that the splitting energy ratio could be adjusted by manipulating the two polarization states separately.

From this example, the lattice constants of the unit cell are set to 150 μm for both directions, which is chosen to be slightly less than the half of wavelength to avoid the diffraction effect. The height of Si unit is set to 195 μm, and this is obtained from the parametric sweeping by commercial FDTD simulator. The phase profile is obtained from the resonance contribution of each Si unit cell, and the height of the unit should be enough to cover 2π phase modulation and efficient transmission.

3.3 Metalens with high efficiency and numerical aperture

An imaging system normally requires a high numerical aperture with enough efficiency to meet the requirement on the resolution and image contrast.

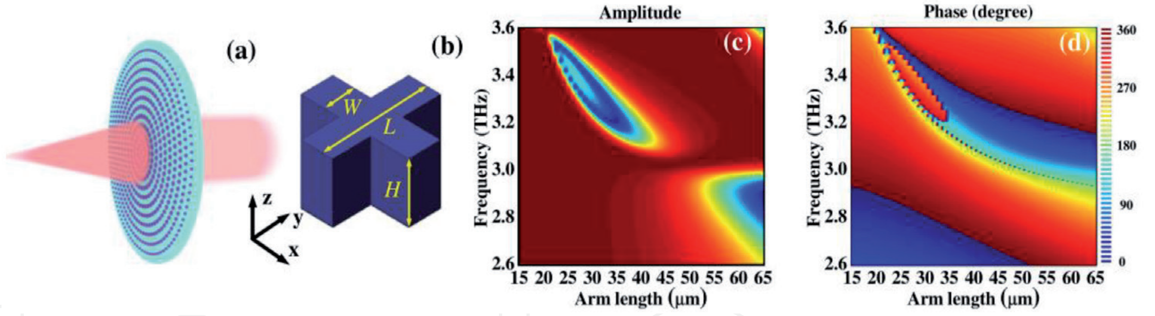

Figure 8.
(a) Schematic of the THz metalens. (b) Schematic of the silicon cross resonators with the incident THz field propagating along z direction and electric field along x direction. The arm width W and the height H are 12 μm and 20 μm, respectively, by varying the arm length L. (c) Transmission amplitudes and (d) corresponding phases as functions of the arm length of the cross resonator and the frequency.

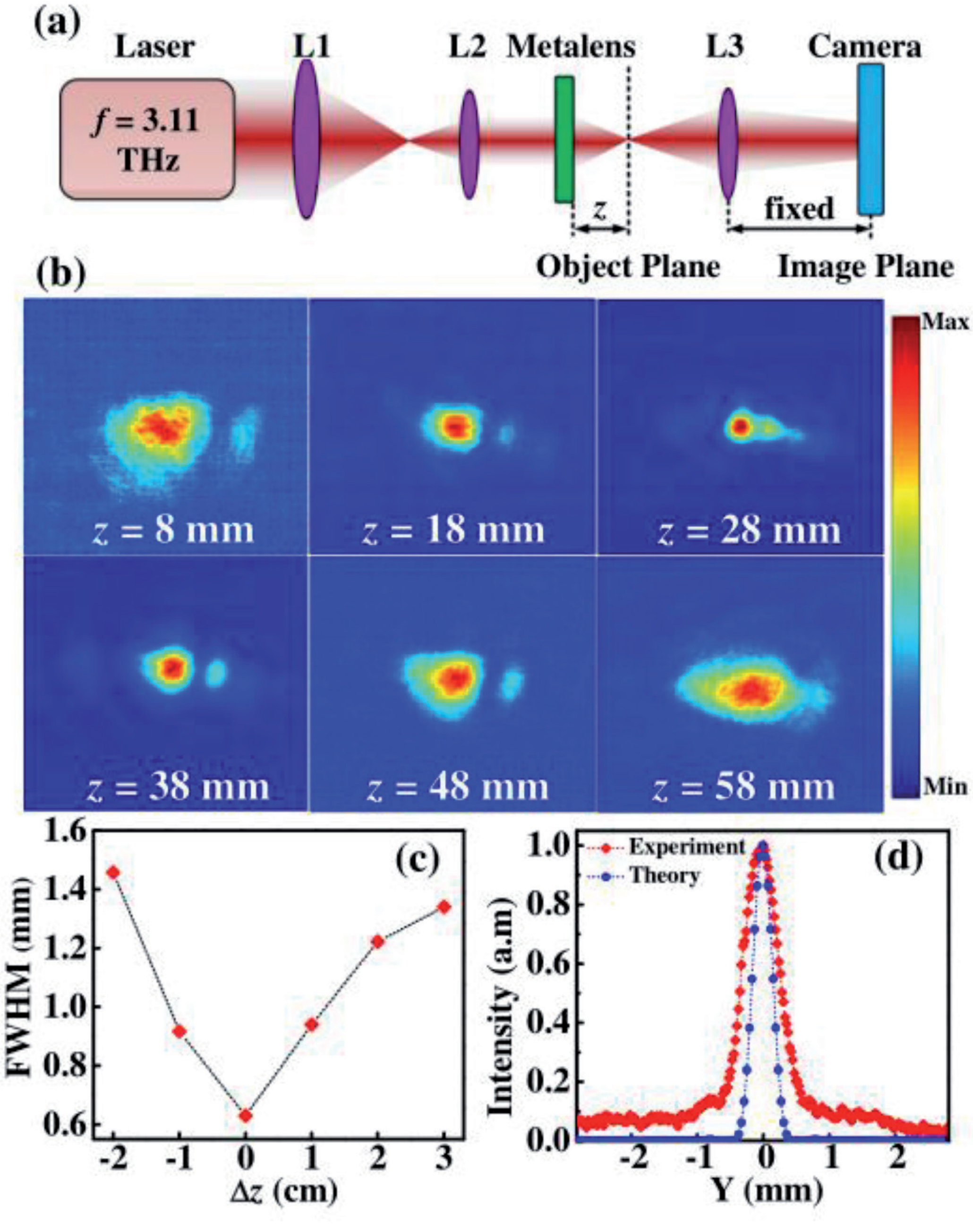

Figure 9.
(a) Setup schematic of the THz metalens imaging experiment. (b) Measured field distribution plane along z direction parallel to the metalens plane. (c) FWHMs of the focus spots along z direction and Δz represent the different distances from the focal plane. (d) Normalized experimental curve in red and theoretical curve in blue indicate the intensity profiles along the y direction at the focal plane.

However, those two factors are usually the critical design trade-offs for the designer. As illustrated in **Figure 8(a)**, the presented THz metalens model consists of a subwavelength silicon resonator array with a hyperboloidal phase profile [10]. Due to the subwavelength arrangement and negligible coupling between adjacent resonators, we consider only the electro-magnetic response of one resonator by a period of 80 μm, as shown in **Figure 8(b)**. In order to obtain the sufficient phase range, we first study the transmission of the resonator by FDTD simulator. Here, the incident THz field is assumed to be a plane wave, propagating along z direction with the electric field along x direction. The refractive index n of the silicon resonator is 3.4. The width and the height of the cross resonator are 12 μm and 20 μm, respectively, and these geometries were optimized to excite electric and magnetic eigenmodes at the interested frequency. **Figure 8(c)** and **(d)** show the transmission amplitudes and the corresponding phases as functions of the arm lengths of the cross resonators and frequency. It worth to mention that, by varying the arm length, the phases of the transmitted wave can be tuned to any value in 2π, while the transmission amplitudes is able to keep relatively high at a fixed frequency of 3.11THz. Based on the simulated results, eight different cross resonators with nearly equidistant steps of π/4 were selected as building atoms of the metasurface, which is able to fully cover 2π phase range.

Figure 9 shows the setup diagram for the metalens imaging experiment and results. The distance between metalens and object plane could be adjusted along z direction and the measured beam profiles at different distances of z are shown in **Figure 9(b)**. FWHMs of the beam spots at different distances Δz away from the focal plane and normalized experimental and theoretical intensity distributions along the y axis are shown in **Figure 9(d)**. The metalens is fabricated on a SOI substrate composed of the designed group of silicon cross resonators that contain both electric and magnetic dipole modes, which is shown in **Figure 8(a)** and **(b)**. By tweaking on the cross resonators geometrically, the cross-resonance of the two dipoles can be manipulated and the phase of the transmitted wave can be realized over a 2π range with a high transmission rate. With the hyperboloid phase distribution, the laser beam can be focused to a spot at distance of 28 mm with a FWHM of 630 μm. The measured focusing efficiency is 24%, which is relatively higher than the most plasmonic metalens cases. Moreover, this work can also be extended in the design of other planar devices, such as beam deflectors or vortex plates.

3.4 Broadband achromatic metalens

In order to address another major challenge as the dispersion, we give the most popular example on an ultra-broadband, achromatic terahertz metalens which can operate at 0.3THz to 0.8THz. The phase profile of the theoretical design introduced in the Section 2, which agrees well with the phase profile transmitted by the metalens in full wave simulation. Owing to the extremely large etching aspect ratio of 1:25, a large phase compensation are achieved from the library of the unit cell, which obtains a relatively high NA value as 0.385 at the large metalens diameter of D = 10 mm. Moreover, the C-shaped unit elements employed in the design exhibit a more robust phase accumulation than the rectangular structures. The metalens is fabricated on a silicon substrate with several hundred microns thickness, which is highly desirable for integration and miniaturization. The design significantly promotes the development of achromatic meta-devices in terahertz hyperspectral imaging and can be used to investigate the robustness of functional metasurface designs [11, 12] (**Figure 10**).

A metalens device consisting of C-shaped unit cells with NA = 0.385 is fabricated with focal length of 12 mm in a diameter of 10 mm. The transmitted field

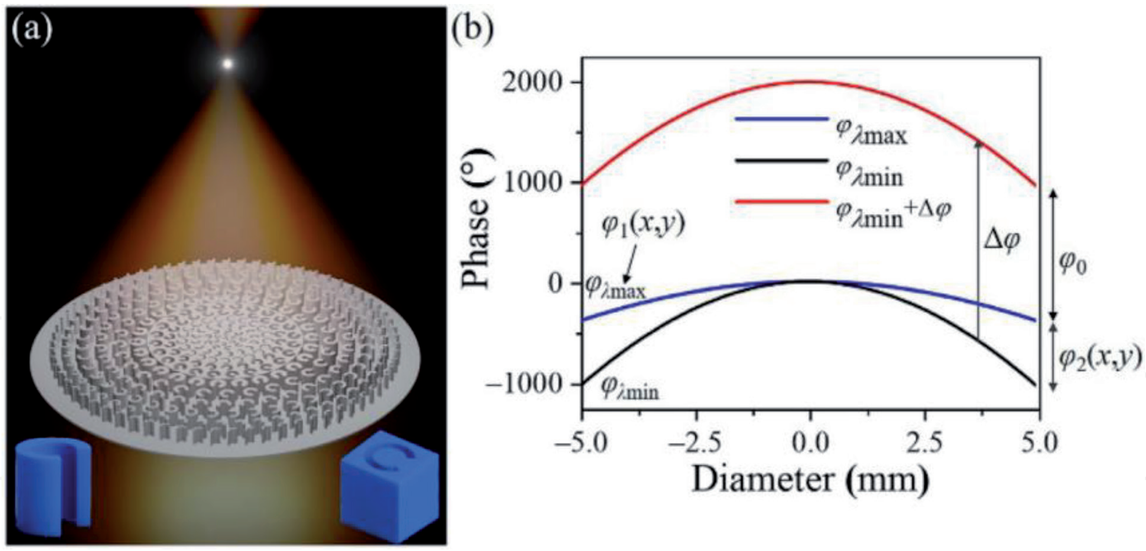

Figure 10.
Schematic of achromatic metalens. (a) Schematic of C-shaped (or rectangular) unit element-based achromatic metalens. (b) Phase profile for achromatic metalens at the wavelength range of λ∈{λmin, λmax}, where Δφ is a certain positive value.

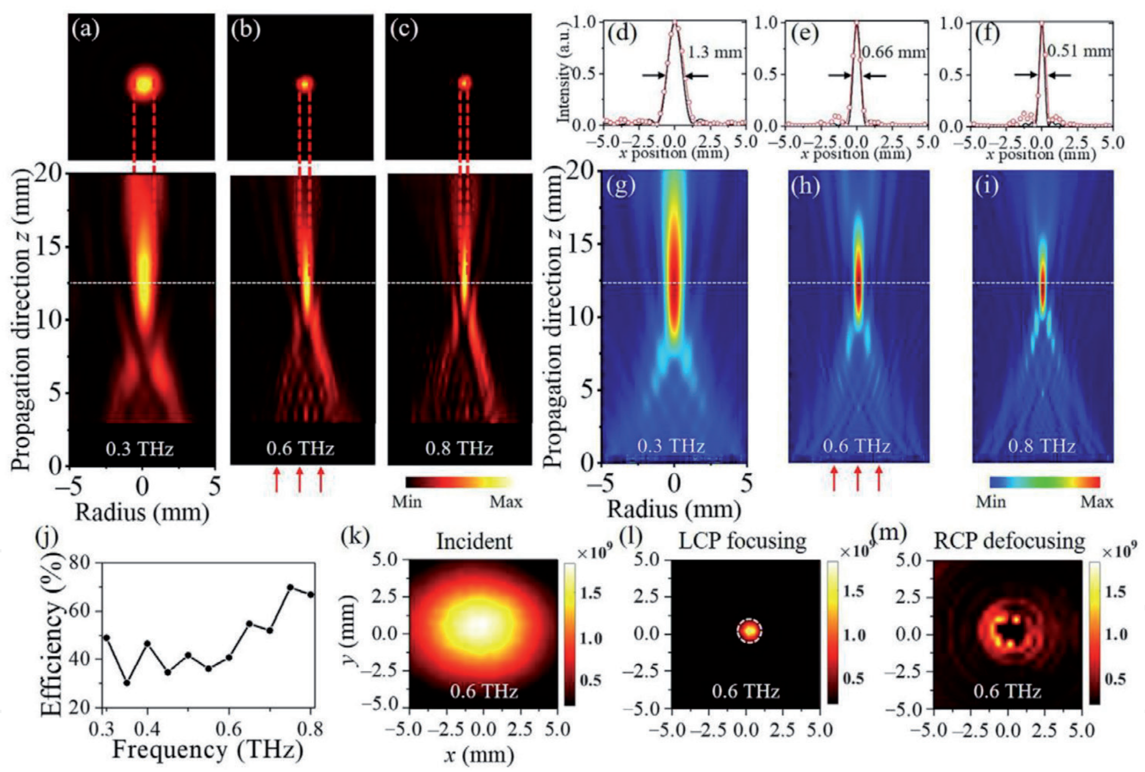

Figure 11.
The focusing demonstration of the achromatic terahertz metalens with C-shaped antenna array. (a)–(c) the intensity profiles at horizontal and vertical cross-sections on the focal plane at the wavelength of 0.3THz, 0.6THz and 0.8THz. (d)–(f) the focal spots profiles obtained from the simulation and experimental results. (g)–(i) simulated results at wavelength of 0.3THz, 0.6THz and 0.8THz. (j) Efficiency trend of the metalens focusing. (k)–(m) incident field, LCP focusing profile and RCP defocusing profile at the wavelength of 0.6THz.

of the horizontal polarization (E_y) on the focal plane is present in **Figure 11a–c**. The experimental results show the high consistence with the simulated results in **Figure 11g–i**, which demonstrates that the focal length at 12 mm shows pretty stable across a broad frequency range. All the measured focus profiles show the full-width at half-maximum (FWHM) close to the diffraction limitation as k/(2NA) shown in **Figure 11(d–f)**. **Figure 11d** shows the horizontal intensity profile at the focal spot for the experimental and numerical results at the terahertz frequency of 0.3THz. The theoretical diffraction limit, k/(2NA), is 1.298 mm, which turns to be close to the experimental result of 1.3 mm. The numerical apertures (NA) of the experimental results at the frequencies of 0.6THz and 0.8THz are NA = 0.385, which matches the designed target as expected.

In general, this example shows that the resonant phase with the geometric phase could be combined to design a high-NA achromatic metalens with C-shaped or rectangular unit cells. The etching depth deviations and shape deformation effect are also considered in the simulation. The experimental results show that the achromatic lens is very close to design target and theoretical diffraction limit and also the durable robustness. The broadband achromatic terahertz metalens already shows the strong potential in some applications such as, hyperspectral imaging, terahertz microscopy.

3.5 Tunable terahertz metalens on graphene

Dynamic tuning is the highly desired feature for a few applications, such as 5G MIMO antenna, imaging radar, free space communication and LiDAR. **Figure 12** shows the stacked graphene metasurface structure proposed in [13]. In this case, the dielectric layers and graphene ribbons are stacked sequentially and the Ag layer is inserted as the rear reflector. The Fermi levels can be realized by adjusting the gate voltages accordingly. **Figure 12(b)** gives a cross-sectional view of a unit cell in this structure. The graphene ribbons period is P = 5 μm and the width is W = 2.9 μm, respectively. The thicknesses are d_2 = 8 μm, d_1 = 13.8 μm for two dielectric layers and the refractive index is n = 1.45. The Ag layer is d_3 = 2 μm and could be treated as the perfect reflector. Due to the reflection from the graphene ribbons and the Ag layer, Fabry–Perot cavity is formed, which is mostly used to boost the resonance between the graphene and the incident light. The incident wave will be chosen to be controlled by one of layers. This feature enables that two-layer graphene structure can effectively control the light by tuning Fermi levels of graphene ribbons from each layer.

Electron beam evaporation technique is used to deposit the Ag film to the substrate and it also is used as the electrodes. Another SiO_2 layer is deposited on the Ag film by plasma enhanced chemical vapor deposition (PECVD). The graphene layer is transferred to the SiO_2 layer and graphene nano-ribbon pattern is etched and formed by electron-beam lithography, which is also another electrode structure shown in **Figure 12(b)**. At last, by repeating the above progress, the stacked graphene metasurface can be implemented (**Figure 13**).

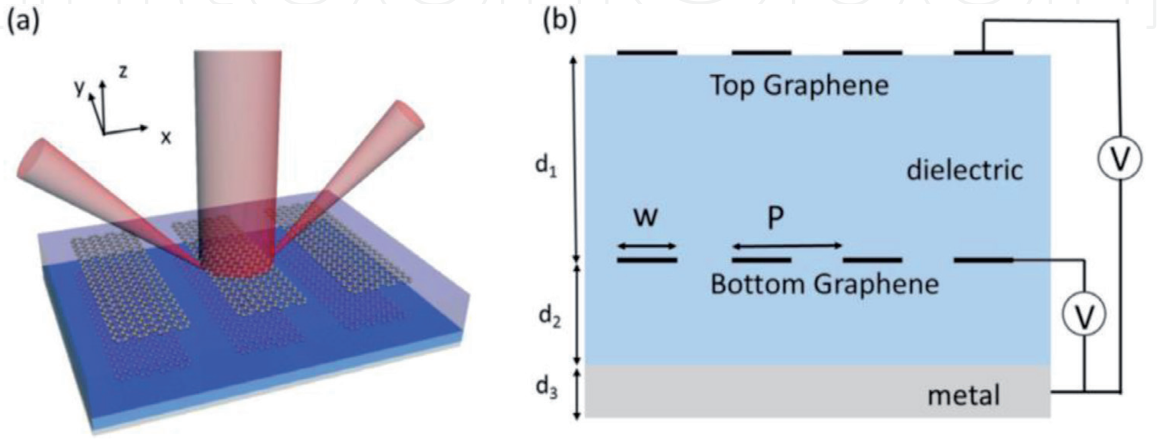

Figure 12.
(a) Schematic of the stacked graphene plasmonic metasurface. (b) the cross-sectional view of the stacked graphene plasmonic metasurface. P is the grating period, and W is the widths of graphene strips. d_1, d_2 and d_3 are the thickness of dielectric layer and Ag layer, respectively.

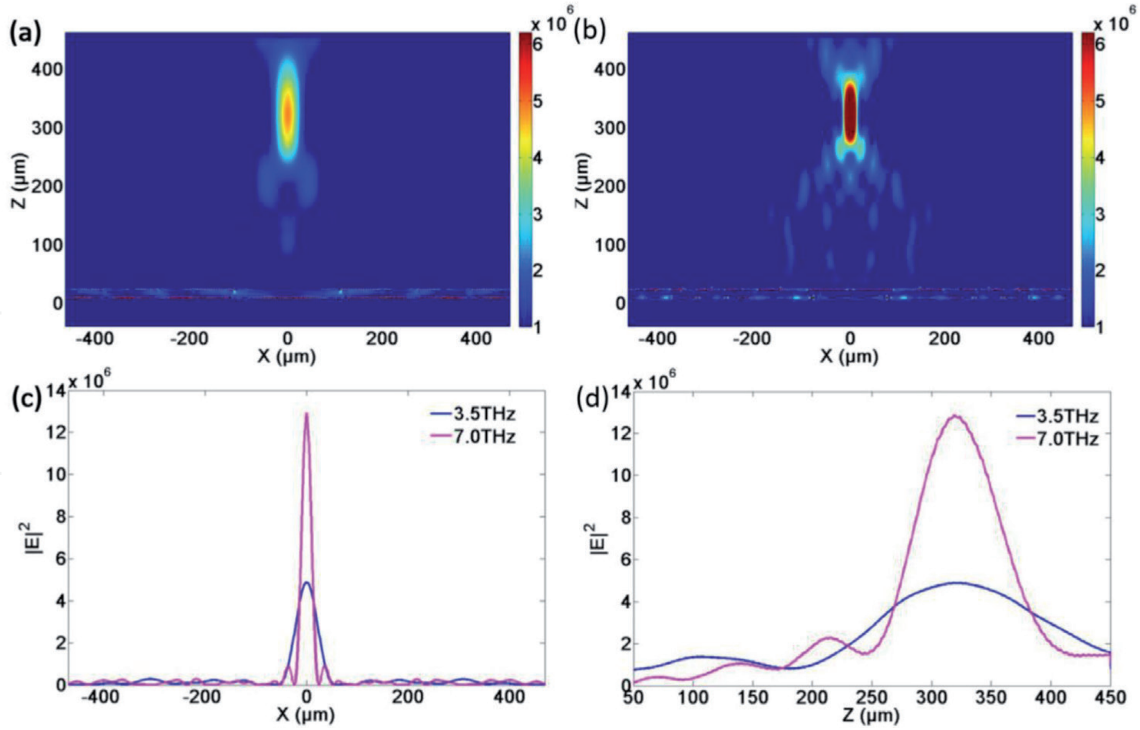

Figure 13.
Intensity distributions of reflective focusing waves from the same metasurface designed under the normal incidences at (a) 3.5THz, (b) 7.0THz. The intensity distributions along the (c) X direction and (d) Z direction at different frequencies.

Normally, the interaction of graphene layer on light is relatively weak since graphene layer only contains single carbon atom layer. It is an issue for most graphene–based devices. In the proposed structure, the stacked graphene structure takes the advantage of Fabry-Perot resonance to achieve multi-band functionality. At one resonant frequency peak, the graphene ribbon layer works as a strong coupler, and other graphene layers are almost transparent. Therefore, in this case, two layers of graphene ribbons can separately tune on optical resonance at different frequencies and there is not strong interference with each other, which is actually extremely difficult to implement by the stacked metal structure. Therefore, the appropriate resonant frequencies should be determined carefully to separate the Fermi levels of the different resonances to isolate the interaction between graphene ribbon layers, since the resonant frequencies of graphene ribbon layers can be independently tuned by Fermi levels in 0-1 eV.

3.6 Liquid crystal tunable terahertz metalens

In this part we give an example of liquid crystal (LC) tunable terahertz lens with spin-selected focusing property [5]. The spin state of LC could be controlled by the external voltage and this case shows how LC is designed and fabricated to function as focus tuning device. The decomposed structure of the device is illustrated in **Figure 14(a)**. Top and bottom substrates are both 800-μm-thick fused silica. With ultrasonically cleaning process, the substrates are transferred with grapheme thin layer and the alignment layer sulfonic azo dye is spin coated onto the grapheme layer. Then the substrates are assembled and separated by Mylar spacer 250 μm away. The dynamic micro-lithography technique using the digital micro-mirror device is introduced to control the spatial distribution of LC directors to implement the desired phase distribution shown in **Figure 14(c)**. Finally, implemented LC orientation profile shown in **Figure 14(b)** agrees well with the design target in **Figure 14(c)** after an LC NJU-LDn-4 is injected with the birefringence over 0.3 from 0.5THz to 2.0THz (**Figure 15**).

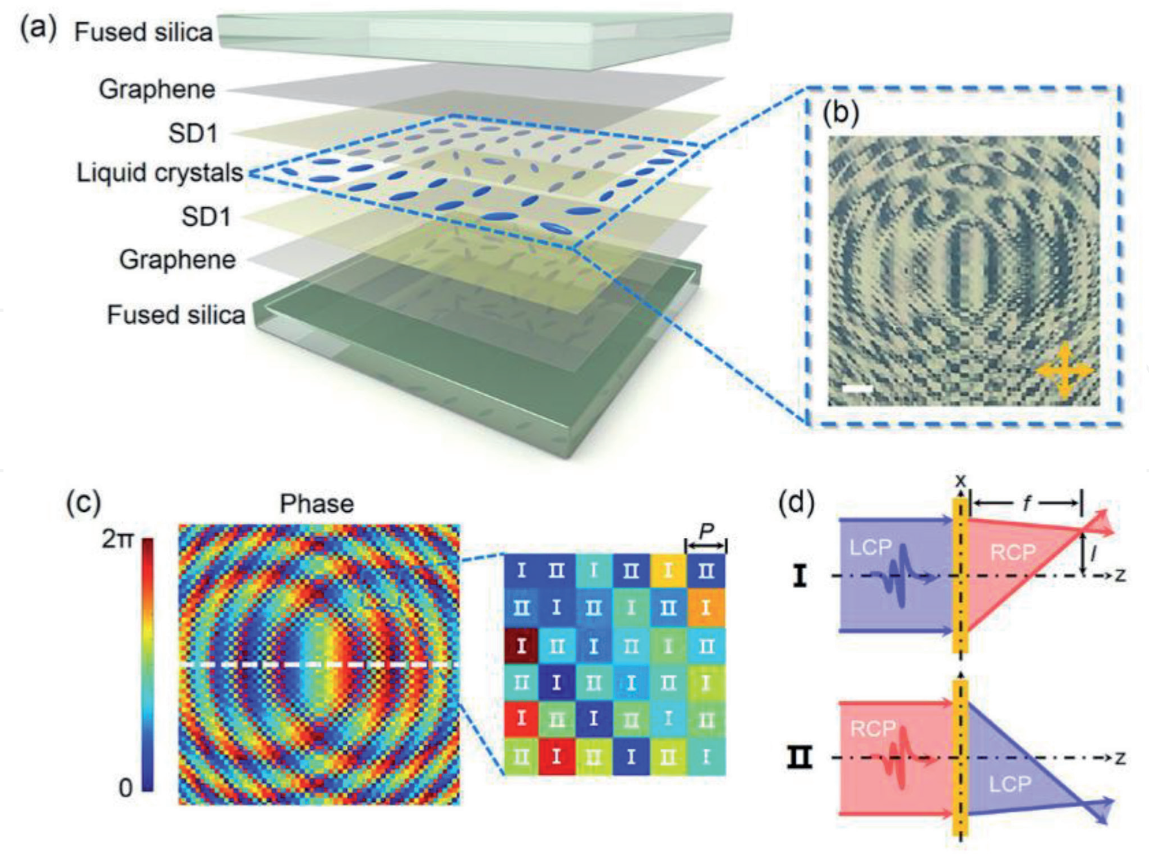

Figure 14.
(a) The schematic of the LC spin-selected flat lens. (b) the photo of the metalens with crossed polarizers incidence in yellow. Scale bar: 1 mm. (c) the designed phase profile. Enlarged part shows a 6 × 6 pixel array, which is composed of lattice I and II with the periodicity p = 152 μm. (d) the focusing effects of mode I and mode II.

3.7 Imaging with terahertz metalens

In this example, we try to give imaging metalens device with a simple structure. To design a practical metalens device for THz imaging application, a simple all-dielectric structure was proposed to distribute the wavefronts with 2π phase-modulation range. **Figure 16** shows the structure that the metasurface unit cell is a silicon cube sitting on top of a Si substrate, and a SiO2 thin layer is inserted in between. The unit cell size is 46.9 μm × 46.9 μm and the width of the cube W is 10.7 μm, the length L is 38.7 μm, and the thickness t is 80 μm [14–16] (**Figures 17**–**20**). A scanning near-field THz microscope (SNTM) setup in **Figure 15** is built to characterize the focusing effect of the metalens, which is made of THz photoconductive generation and probe detection. The THz field intensity in the x-y and x-z plane from 0.8 to 1.2THz for LP, LCP and RCP waves are shown in **Figure 15**(**b-d**) LCP wave is focused to left of z-axis and RCP wave is focused to the right of z-axis. The experimental results match well with the simulation.

This example gives the experimental result of THz imaging with a linear polarized, all-dielectric metalens. The structure of metalens is quite simple and feasible to a CMOS compatible platform for the practical implementation. The Engraved character gratings on the substrate have been tested and the result indicates that image resolution by this design is close to λ.

3.8 Polarization controllable metamaterial absorber at terahertz frequency

Metamaterial Absorbers (MA) is another primary application to tune on the polarization of metamaterial to control the absorption [17]. Over the decades there

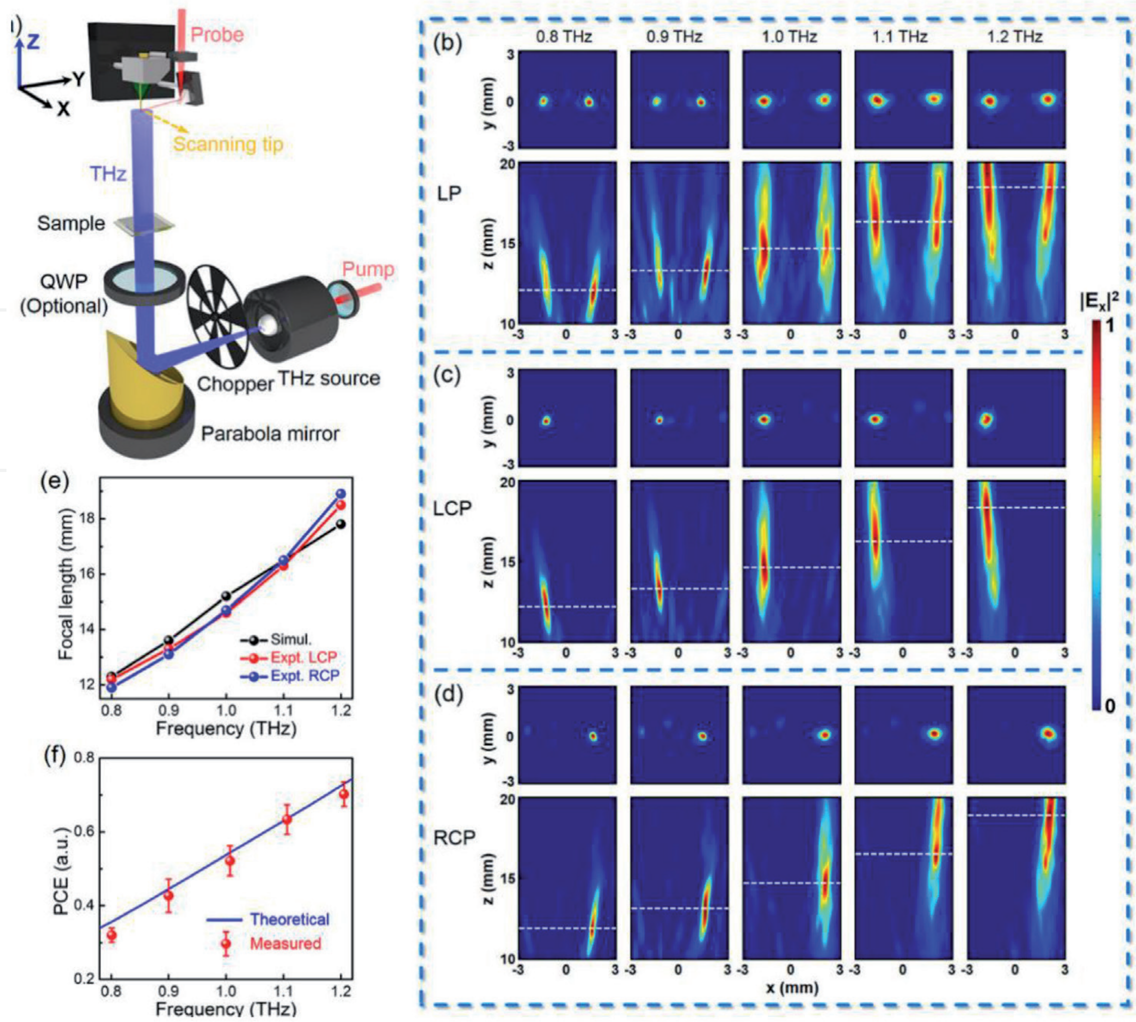

Figure 15.
(a) The schematic of SNTM system setup. (b–d) Measured THz field intensity in xz-plane and the focal planes from 0.8THz to 1.2THz for the incident wave of (b) LP, (c) LCP and (d) RCP. (e) The relationship of focal length with frequency for LCP and RCP case. (f) The relationship of PCE with frequency.

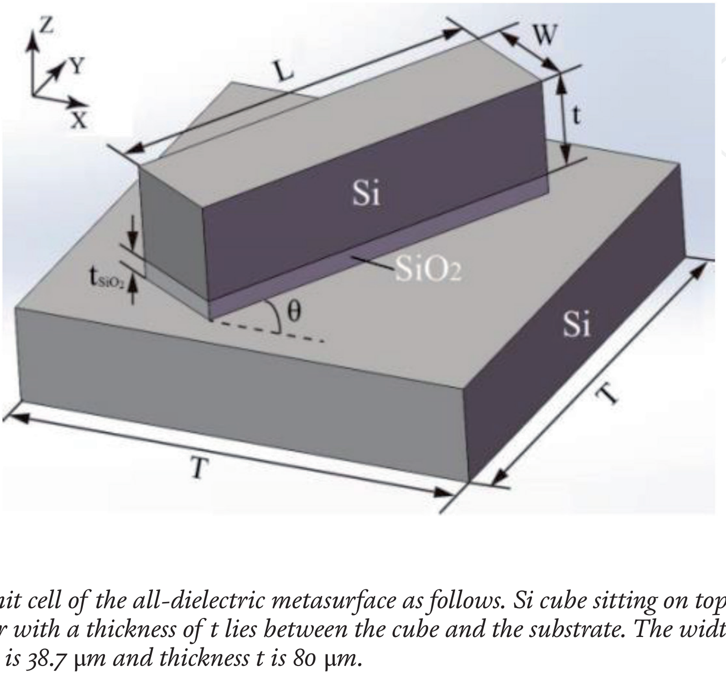

Figure 16.
46.9 μm × 46.9 μm unit cell of the all-dielectric metasurface as follows. Si cube sitting on top of a Si substrate and a thin SiO2 layer with a thickness of t lies between the cube and the substrate. The width W of the cube is 10.7 μm, the length L is 38.7 μm and thickness t is 80 μm.

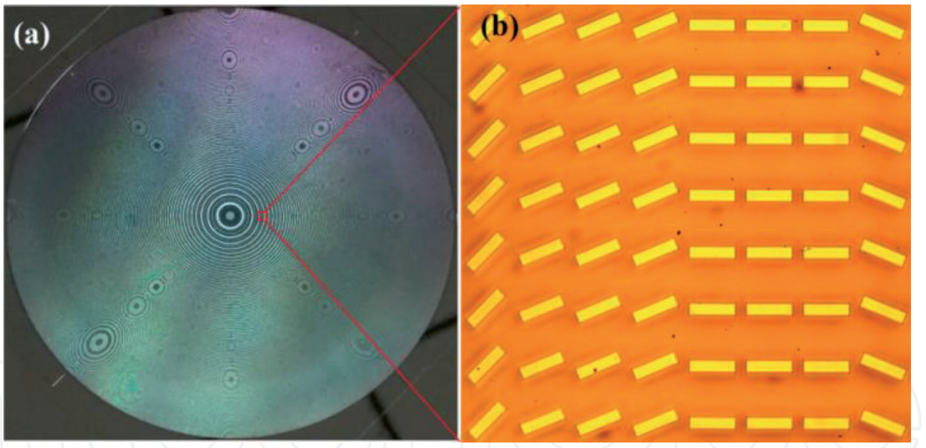

Figure 17.
(a) Photograph of the metalens device based on all-dielectric metasurface; (b) optical microscope image of central area of metalens.

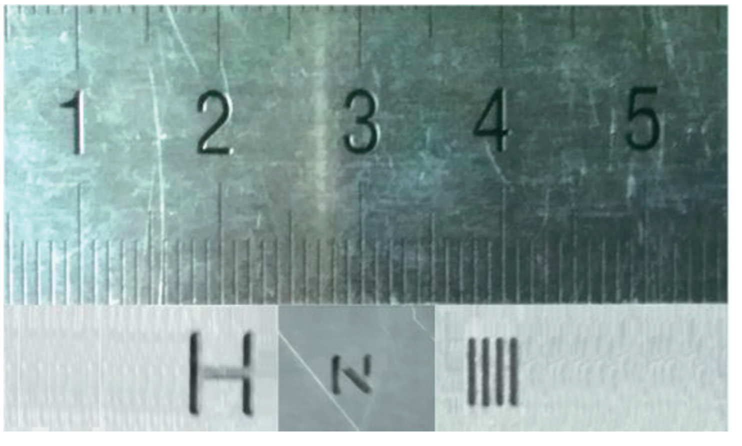

Figure 18.
Targets used in imaging experiments, including letters "H" and "N," and a piece of grating with linewidth of 0.5 mm.

has been a huge amount of research about Metamaterial Absorbers achieving high absorption and also multi-absorption peaks with split-ring resonator, U-shape, T-shape, hexagon-shape and so on. In this example the polarization controllable dual-band MA is given as follow. The absorber consists of one substrate with two pairs of metallic strips at the top, where two horizontal strips and vertical strips are grouped together to sweep the length to tune on the resonance peaks for different polarizations. Results show that the two perfect absorption peaks could be obtained for x-polarization, and two absorption peaks with an average absorbance of 97.28% can be obtained for y-polarization. The near-field distributions at resonating frequency are also investigated for polarization controllable dual-band absorption. The results show that polarization insensitive dual-band MA can be feasible with the all strips lines having the same length [18–20].

The design details of dual-band polarization controllable MA are shown in **Figure 21**. **Figure 21(a)** and **(b)** show the skeptical side view and the top view of device. The three-layer sandwich structure is utilized to obtain the desired absorption along x and y polarizations, which are marked as A, B, C, and D, respectively. The strips A and B have the length of 130 μm, and strips C and D have the length of 100 μm. The distance between the center of two strips pairs and the unit cell center is labeled as δ_1 = 15 μm and δ_2 = 15 μm. Simulation results show that the four strips have the same width of w = 10 μm, while the lengths along different polarizations are different. This metamaterial-based structure could be very useful for the switching, controlling the broadband absorption for terahertz device.

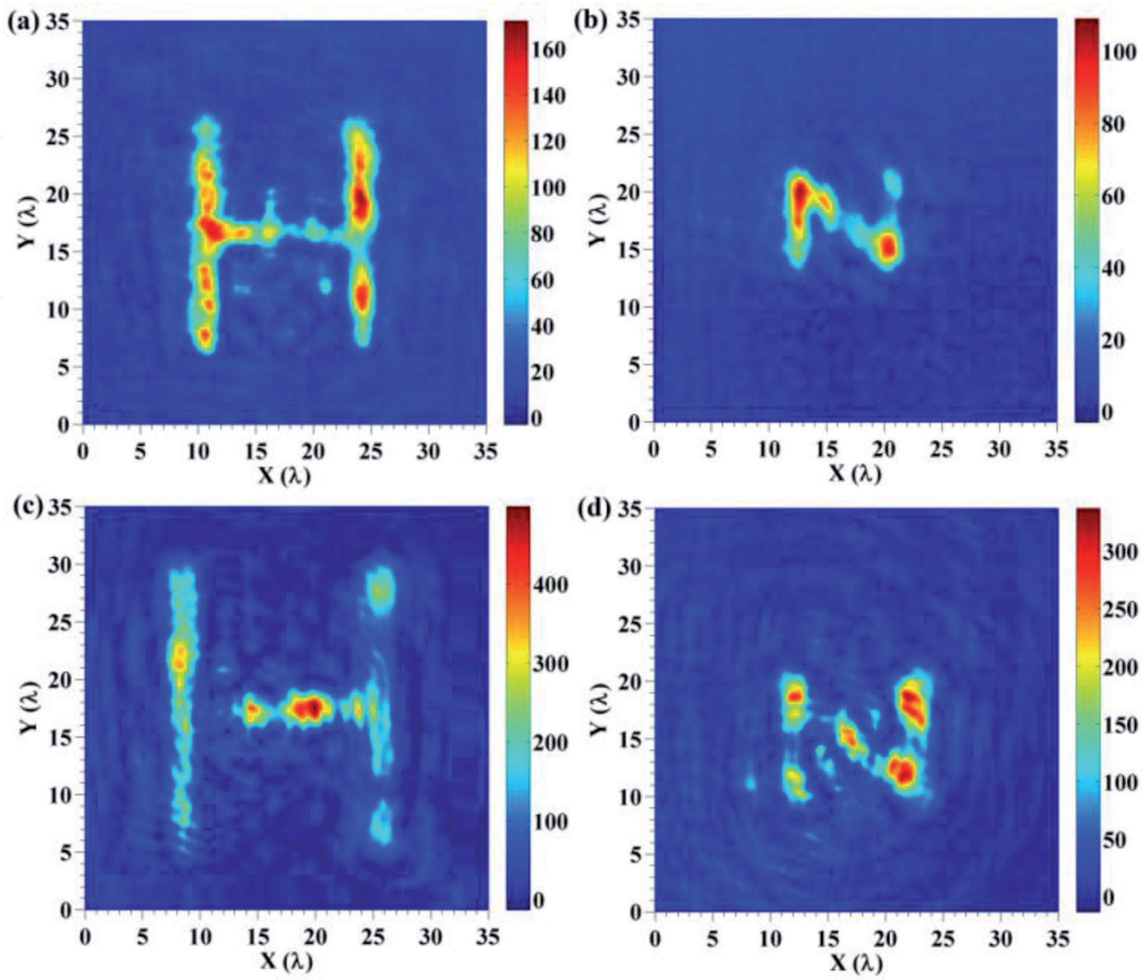

Figure 19.
Imaging results with incidence of a linearly polarized THz wave at wavelength of 118.8 μm. Measured images of letters (a) "H" and (b) "N" when the metalens top side faces the targets, and measured images of letters (c) "H" and (d) "N" when the metalens substrate side faces the targets.

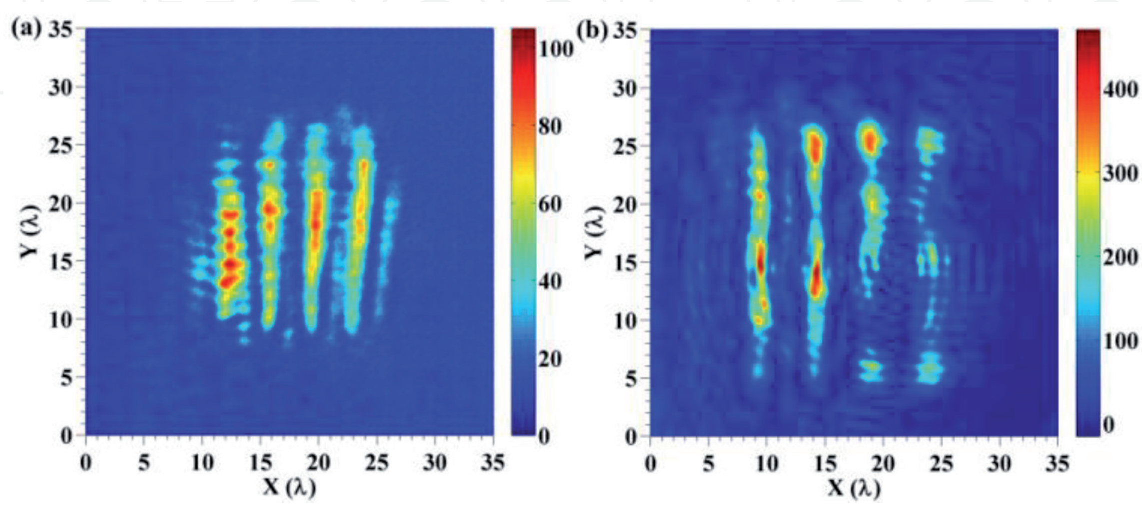

Figure 20.
Imaging results with incidence of a linearly polarized THz wave at wavelength of 118.8 μm for (a) when the lens metasurface top side faces the grating, and (b) when the metalens substrate side faces the grating.

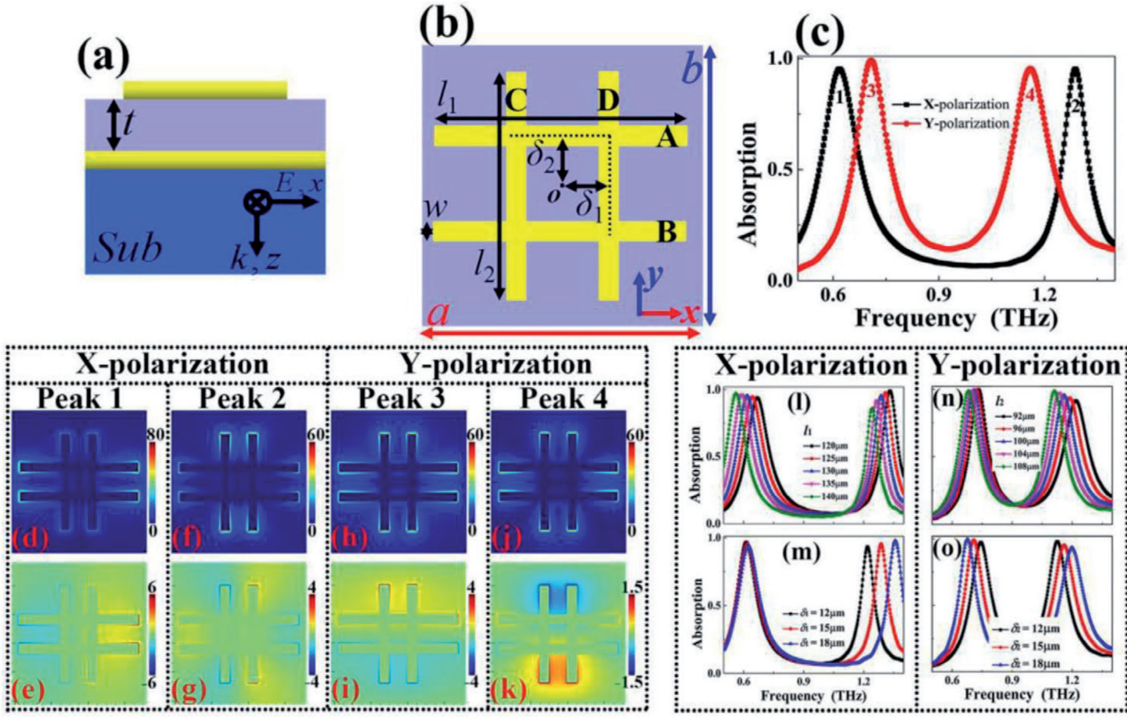

Figure 21.
(a) The structure of dual-band polarization controllable MA absorber; (b) two pairs of metallic strips at the top of structure; (c) absorption curves along the x-polarization and y-polarization; (d) and (f) are the E fields of the two peaks along x-polarization; (e) and (g) are the Ez fields of the two peaks along x-polarization; (h) and (j) are the |E| fields of the two peaks along y-polarization; (i) and (k) are the Ez fields of the two peaks along y-polarization; absorption spectrum with the variations of the l_1(l) and δ_1(m) along x-polarization; absorption spectrum with the variations of the l_2 (n) and δ_2 (o) along y-polarization.

4. Conclusion

So far metamaterial has stimulated a lot of revolutionary work in the traditional microwave antenna technology. Some typical applications such as 5G MIMO antenna, metamaterial absorber, and polarization controllers are already been used for telecommunications and imaging radar. Worth to mention that, in the booming area of high frequency applications like terahertz and optical regime, metalens is definitely more attractive subject, since the stronger bandwidth capacity and high resolution at high frequency will pave the way for countless more opportunities in the field of the high-speed communications, secure imaging, bio-medical sensing and novel microscopy [21, 22]. In this chapter, we have reviewed the design principle as the general routine and elaborate the focalization and beamforming effect. The content covers the broad range of application cases from microwave front-end antenna to optical achromatic imaging lens. However, the metamaterial is still a fast-paced and highly interdisciplinary area. Some cutting-edge technologies like the inverse deep-learning method are used to design the metalens for large aperture, achromatic and efficient focusing. The liquid crystal metamaterials (LCM) have been created for large-angle beamforming of microwave, and potentially infrared Laser for solid-state LiDAR technology.

Acknowledgements

This work was supported by the National Natural Science Foundation of China (#61975228), Pilot AI company and Soleilware LLC.

Author details

Qi Song[1*], Yan Gong[1], Nianxi Xu[2] and Ruoqian Gao[1]

1 Suzhou Institute of Biomedical Engineering and Technology, Chinese Academy of Sciences, Suzhou, China

2 Changchun Institute of Optics, Fine Mechanics and Physics, Chinese Academy of Sciences, Changchun, China

*Address all correspondence to: songq@sibet.ac.cn

References

[1] R.Q Gao, Q Song, H Liu, J.B Gao, X.Y Wang, Bayanheshig, Design of near-Infrared reconfigurable metalens on Silicon-On-Insulator (SOI) platform with Fabry-Perot phase shifter, Optics Communications 466 (C), 56-63

[2] TJ Cui, MQ Qi, X Wan, J Zhao, Q Cheng, Coding metamaterials, digital metamaterials and programmable metamaterials, Light: Science & Applications 3 (10), e218-e218

[3] RQ Gao, Q Song, JB Gao, H Liu, XY Wang, XH Chen, JS Gao A novel design method of large-aperture metalens and investigation of electrical focus-tuning mechanism with phase shifter structures, SPIE/COS Photonics Asia, 2018, Beijing, China

[4] D. Jia, Y. Tian, W. Ma, X. Gong, J. Yu, G. Zhao, X. Yu, Transmissive terahertz metalens with full phase control based on a dielectric metasurface, Optics Letters, 42 (2017) 4494-4497.

[5] Z. Shen, S. Zhou, S. Ge, W. Duan, L. Ma, Y. Lu, W. Hu, Liquid crystal tunable terahertz lens with spin-selected focusing property, Optics Express, 27 (2019) 8800-8807.

[6] Q Song, S Campione, O Boyraz, F Capolino, Silicon-based optical leaky wave antenna with narrow beam radiation, Optics express 19 (9), 8735-8749

[7] S Campione, C Guclu, Q Song, O Boyraz, F Capolino, An optical leaky wave antenna with Si perturbations inside a resonator for enhanced optical control of the radiation, Optics express 20 (19), 21305-21317

[8] J. Jiao, G. Liang, J. Guo, E. Lin, X. Huang, X. Luo, Q. Zhao, Study on focusing properties of broadband range and oblique incidence on the basis of V-shaped nanoantenna, Applied Physics a-Materials Science & Processing, 122 (2016).

[9] J. Zhou, J. Wang, K. Guo, F. Shen, Q. Zhou, Z. Yin, Z. Guo, High-efficiency terahertz polarization devices based on the dielectric metasurface, Superlattices and Microstructures, 114 (2018) 75-81.

[10] J. Wang, J. Zhou, K. Guo, F. Shen, Q. Zhou, Z. Yin, Z. Guo, High-efficiency terahertz dual-function devices based on the dielectric metasurface, Superlattices and Microstructures, 120 (2018) 759-765.

[11] X. Zang, W. Xu, M. Gu, B. Yao, L. Chen, Y. Peng, J. Xie, A.V. Balakin, A.P. Shkurinov, Y. Zhu, S. Zhuang, Polarization-Insensitive Metalens with Extended Focal Depth and Longitudinal High-Tolerance Imaging, Advanced Optical Materials, 8 (2020).

[12] Q. Cheng, M. Ma, D. Yu, Z. Shen, J. Xie, J. Wang, N. Xu, H. Guo, W. Hu, S. Wang, T. Li, S. Zhuang, Broadband achromatic metalens in terahertz regime, Science Bulletin, 64 (2019) 1525-1531.

[13] Z. Yin, Q. Zheng, K. Wang, K. Guo, F. Shen, H. Zhou, Y. Sun, Q. Zhou, J. Gao, L. Luo, Z. Guo, Tunable dual-band terahertz metalens based on stacked graphene metasurfaces, Optics Communications, 429 (2018) 41-45.

[14] X. Xiong, X. Wang, Z. Wang, Y. Gao, R. Peng, M. Wang, Constructing an achromatic polarization-dependent bifocal metalens with height-gradient metastructures, Optics Letters, 46 (2021) 1193-1196.

[15] X. Jiang, H. Chen, Z. Li, H. Yuan, L. Cao, Z. Luo, K. Zhang, Z. Zhang, Z. Wen, L.-g. Zhu, X. Zhou, G. Liang, D. Ruan, L. Du, L. Wang, G. Chen, All-dielectric metalens for terahertz wave imaging, Optics Express, 26 (2018) 14132-14142.

[16] H.-H. Tang, P.-K. Liu, Terahertz metalenses for evanescent wave focusing and super-resolution imaging, Journal of Electromagnetic Waves and Applications, 29 (2015) 1776-1784.

[17] B.-X. Wang, Y. He, N. Xu, X. Wang, Y. Wang, J. Cao, Design of dual-band polarization controllable metamaterial absorber at terahertz frequency, Results in Physics, 17 (2020).

[18] B.-X. Wang, Y. He, P. Lou, N. Xu, X. Wang, Y. Wang, J. Cao, Multiple-Band Terahertz Metamaterial Absorber Using Multiple Separated Sections of Metallic Rectangular Patch, Frontiers in Physics, 8 (2020).

[19] Y. He, B.-X. Wang, P. Lou, N. Xu, X. Wang, Y. Wang, Resonance Bandwidth Controllable Adjustment of Electromagnetically Induced Transparency-like Using Terahertz Metamaterial, Plasmonics, 15 (2020) 1997-2002.

[20] Y. He, B.-X. Wang, P. Lou, N. Xu, X. Wang, Y. Wang, J. Cao, Convert from Fano resonance to electromagnetically induced transparency effect using anti-symmetric H-typed metamaterial resonator, Optical and Quantum Electronics, 52 (2020).

[21] F Qian, Q Song, EK Tien, SK Kalyoncu, Y Huang, O Boyraz, Effects of design geometries and nonlinear losses on gain in silicon waveguides with erbium-doped regions, IEEE Journal of Quantum Electronics 47 (3), 327-334

[22] Q Song, F Qian, EK Tien, I Tomov, J Meyer, XZ Sang, O Boyraz, Imaging by silicon on insulator waveguides, Applied Physics Letters 94 (23), 231101